Nanoscale

COMMUNICATION

View Article Online
View Journal | View Issue

Tailoring pore structures with optimal mesopores to remarkably promote DNA adsorption guiding the growth of active $Mn_3(PO_4)_2$ toward sensitive superoxide biomimetic enzyme sensors

Zhuo Zou,[a,b] Xiao Qing Ma,[a,b] Long Zou,[c] Zhuan Zhuan Shi,[a,b,d] Qiang Qiang Sun,[a,b] Qian Liu,[a,b] Tao Tao Liang[a,b] and Chang Ming Li *[a,b,d]

[a]*Institute for Clean Energy & Advanced Materials, Southwest University, Chongqing 400715, P.R. China. E-mail: ecmli@swu.edu.cn*

[b]*Chongqing Key Laboratory for Advanced Materials and Technologies of Clean Energies, Chongqing 400715, P.R. China*

[c]*College of Life Sciences, Jiangxi Normal University, Nanchang 330022, China*

[d]*Institute for Materials Science and Devices, Suzhou University of Science and Technology, Suzhou 215011, P.R. China*

Accepted 21st December 2018

DOI: 10.1039/c8nr08829b

Tanvi Gupte

21.12.2019

Introduction

- The superoxide anion ($O_2^{\cdot -}$) is a reactive oxygen species (ROS), and also a precursor to produce other ROS such as hydrogen peroxide (H_2O_2) and the hydroxyl radical ($^{\cdot}OH$).
- It is of great importance to sensitively monitor *in situ* $O_2^{\cdot -}$ released from cells for health screening, disease diagnosis and pathological study.
- Electrochemical $O_2^{\cdot -}$ sensors mainly rely on specific enzymes such as superoxide dismutase and Cytochrome *c*, but the sensors often suffer from poor reproducibility, short shelf time and high expense.
- Why porous electrode?
  - Large surface area = high sensitivity
  - Inner pore surface can be modified to improve surface adsorptions or trapping of specific target molecules

Schematic illustration of the formation of $Mn_3(PO_4)_2$–DNA/CNFs.

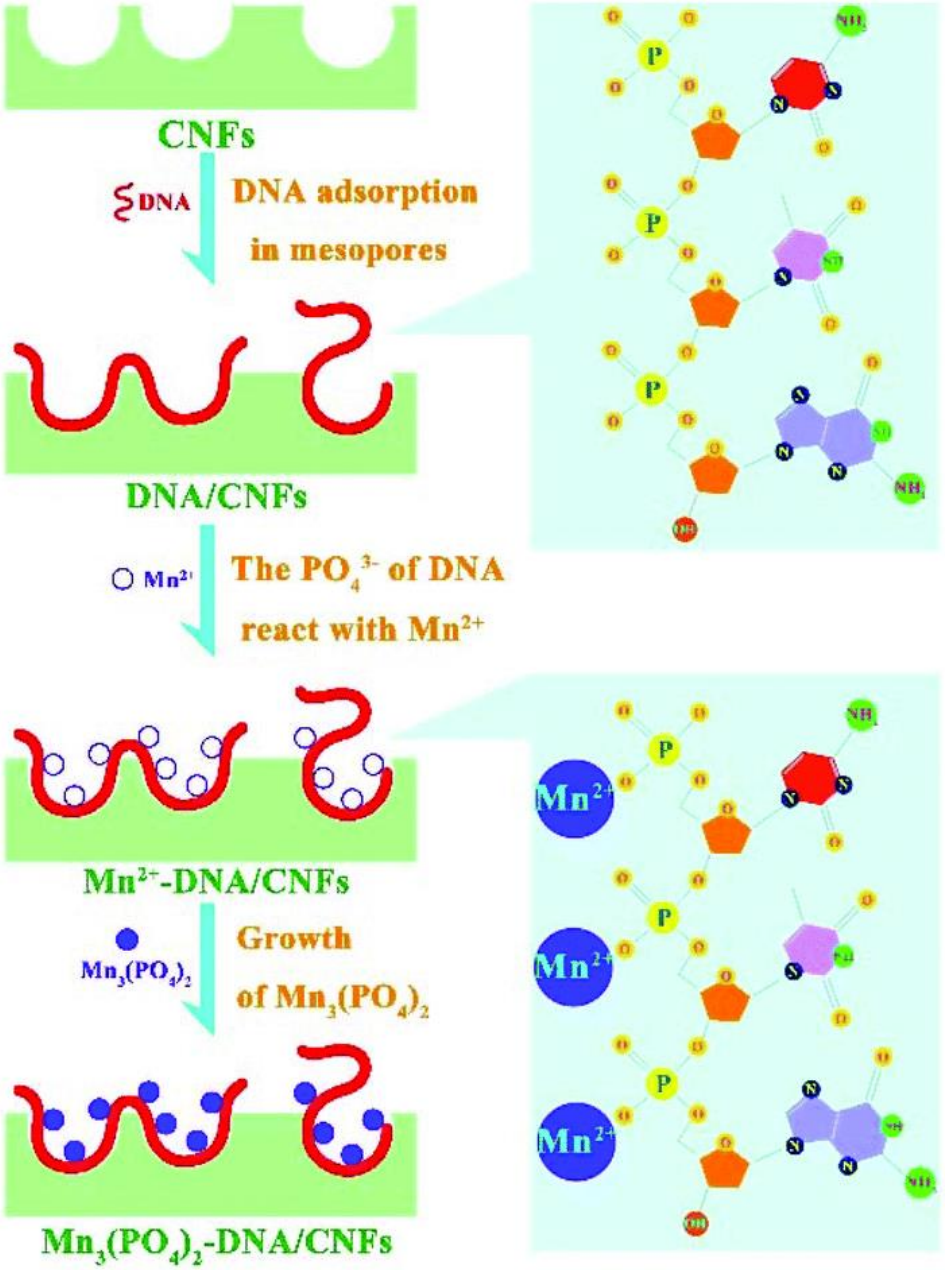

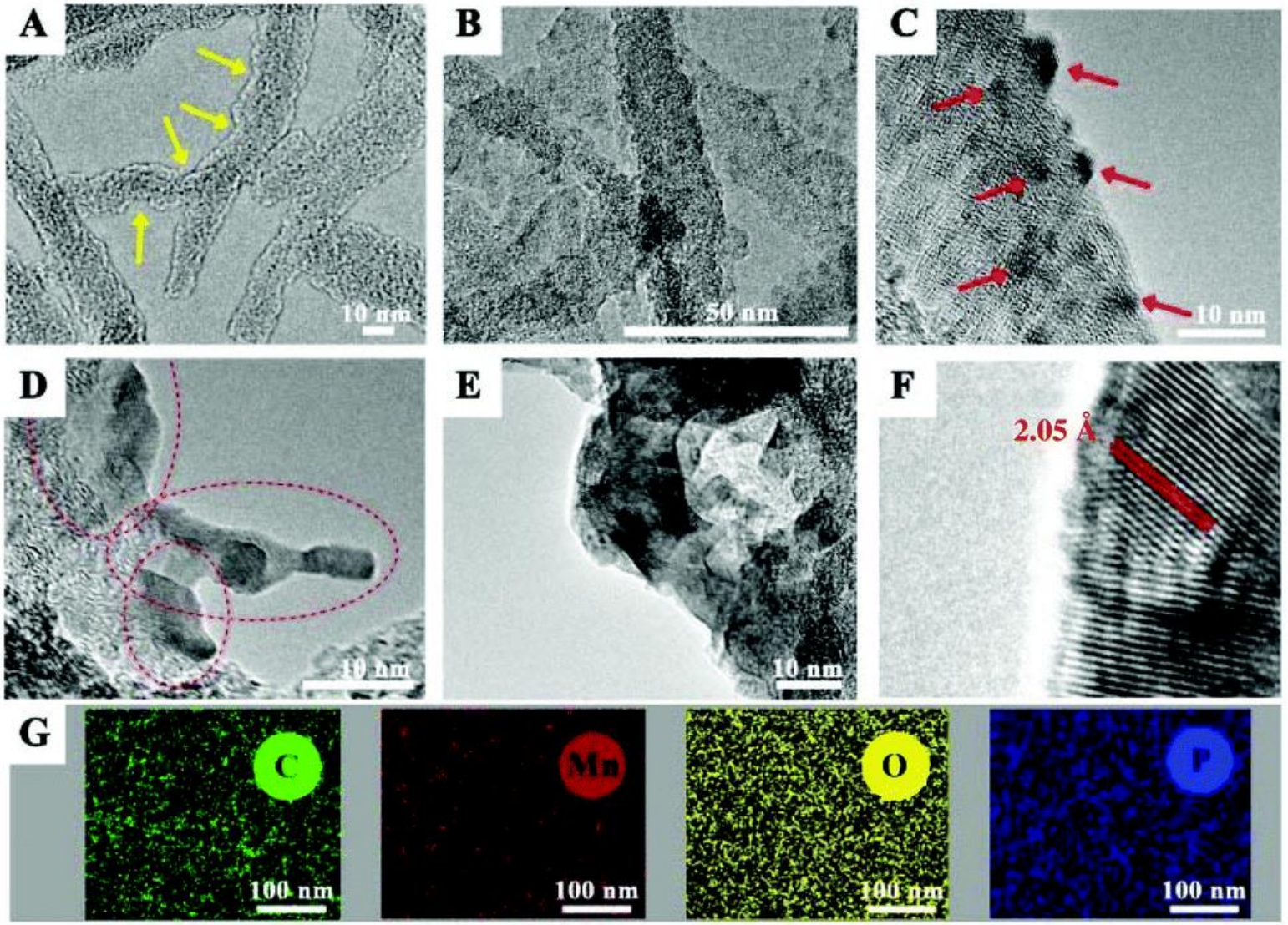

TEM images of (A) CNFs and (B, C, D and E) $Mn_3(PO_4)_2$–DNA/CNFs, (F) HRTEM of $Mn_3(PO_4)_2$–DNA, and (G) the element area profiles of C, Mn, O and P elements in the as-prepared $Mn_3(PO_4)_2$–DNA/CNFs.

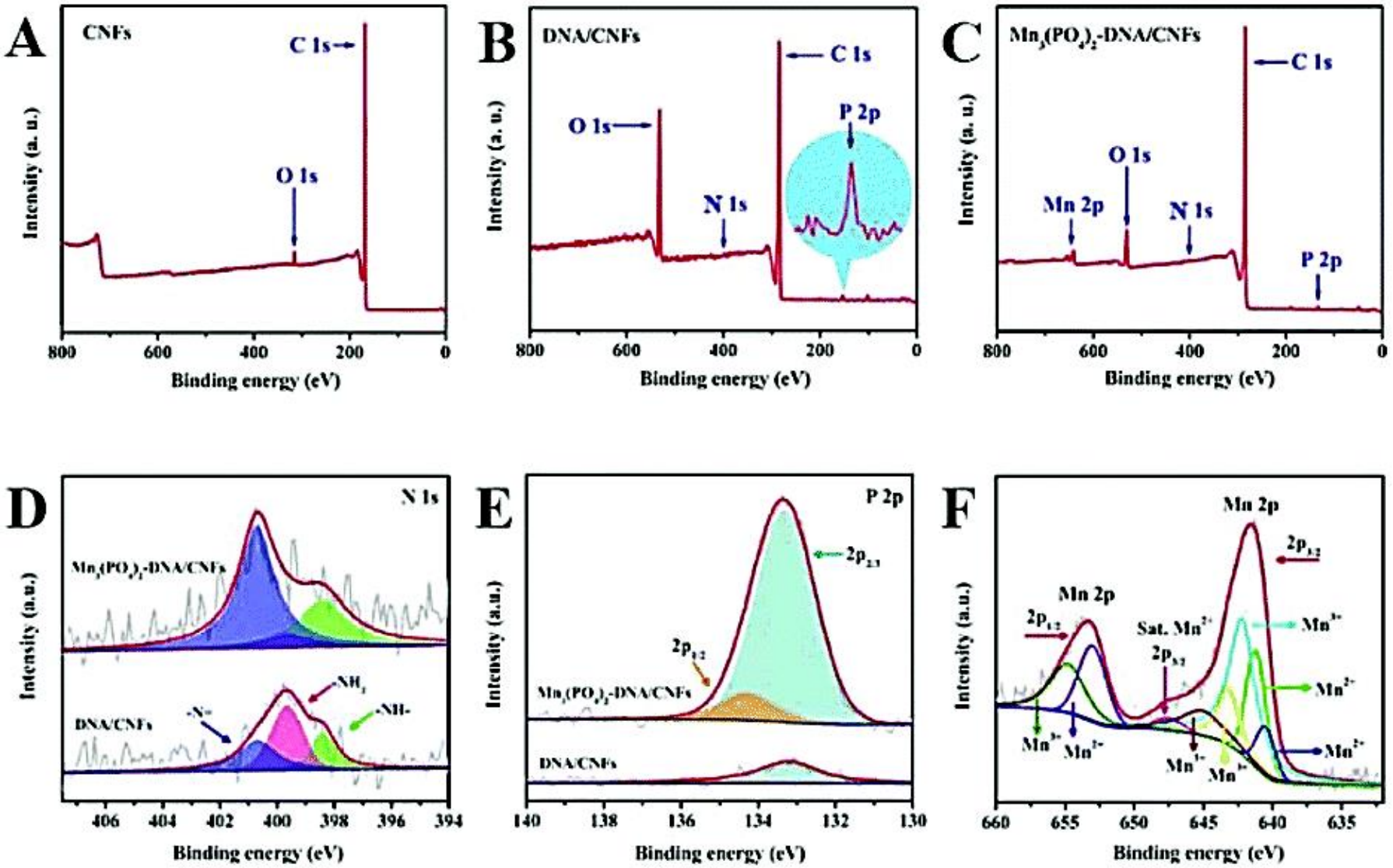

XPS analysis of (A) variation of the composition of functionalized CNFs, (B) wide scan survey spectra of DNA/CNFs, (C) wide scan survey spectra of $Mn_3(PO_4)_2$–DNA/CNFs, (D) N 1s spectra in DNA/CNFs and $Mn_3(PO_4)_2$–DNA/CNFs showing three peaks for amine group (398.4 eV) and nonconjugated N sp 3 (399.64 and 400.7 eV) belonging to the cytosine-base oligomer., (E) P 2p spectra in DNA/CNFs and $Mn_3(PO_4)_2$–DNA/CNFs, and (F) Mn 2p spectra in $Mn_3(PO_4)_2$–DNA/CNFs.

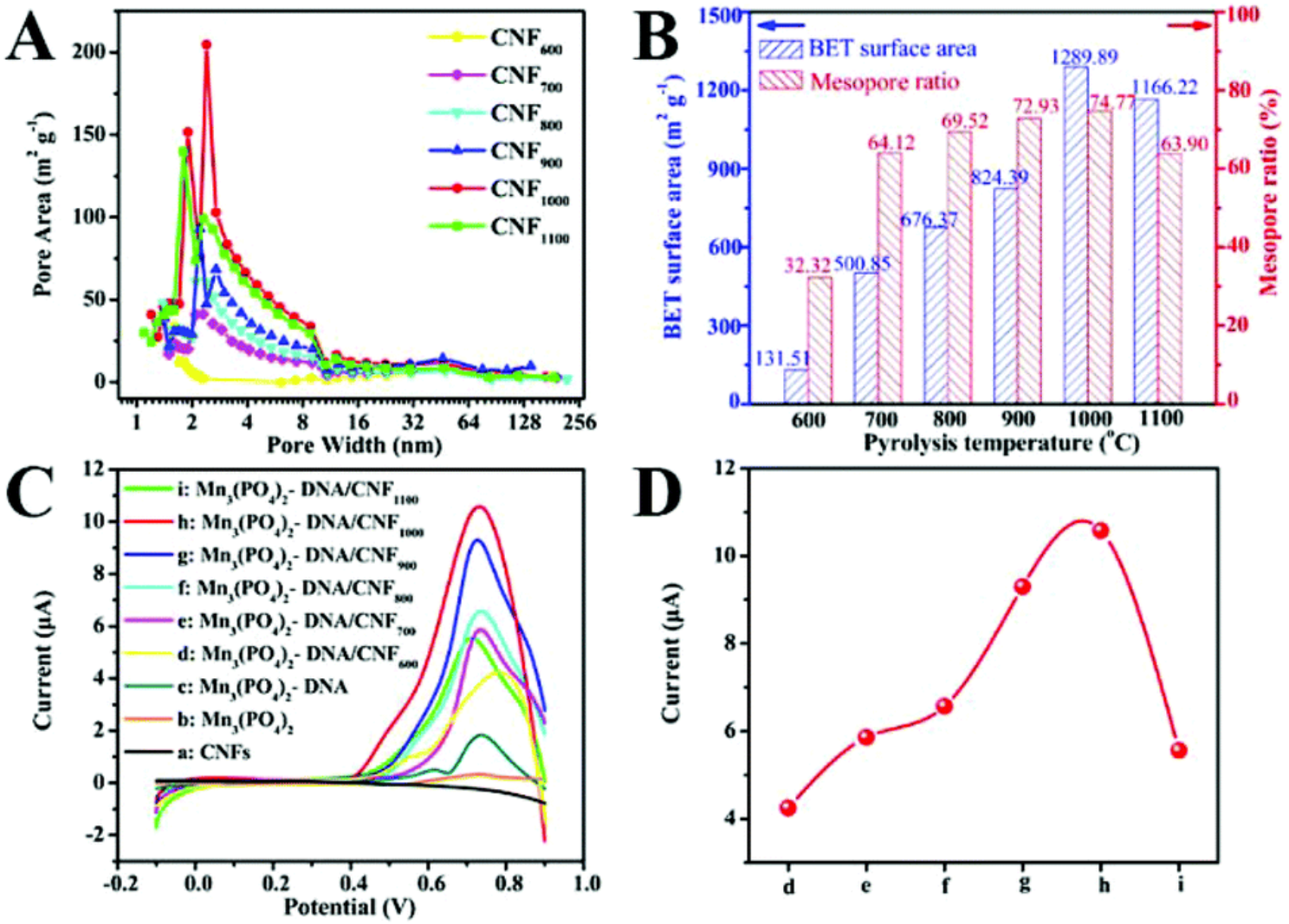

(A) The pore size distribution curves of CNFs, (B) the BET surface areas and the mesopore ratio of CNFs, (C) CVs with a substrate background obtained with different material modified GCEs toward 1 μmol L^{-1} $O_2^{\cdot -}$ in PBS solution. (Curve a) CNFs, (curve b) $Mn_3(PO_4)_2$, (curve c) $Mn_3(PO_4)_2$–DNA, (curve d) $Mn_3(PO_4)_2$–DNA/CNF_{600}, (curve e) $Mn_3(PO_4)_2$–DNA/CNF_{700}, (curve f) $Mn_3(PO_4)_2$–DNA/CNF_{800}, (curve g) $Mn_3(PO_4)_2$–DNA/CNF_{900}, (curve h) $Mn_3(PO_4)_2$–DNA/CNF_{1000}, (curve i) $Mn_3(PO_4)_2$–DNA/CNF_{1100}, and (D) relationship of the peak currents of $Mn_3(PO_4)_2$–DNA on different CNF modified GCEs according to (C).

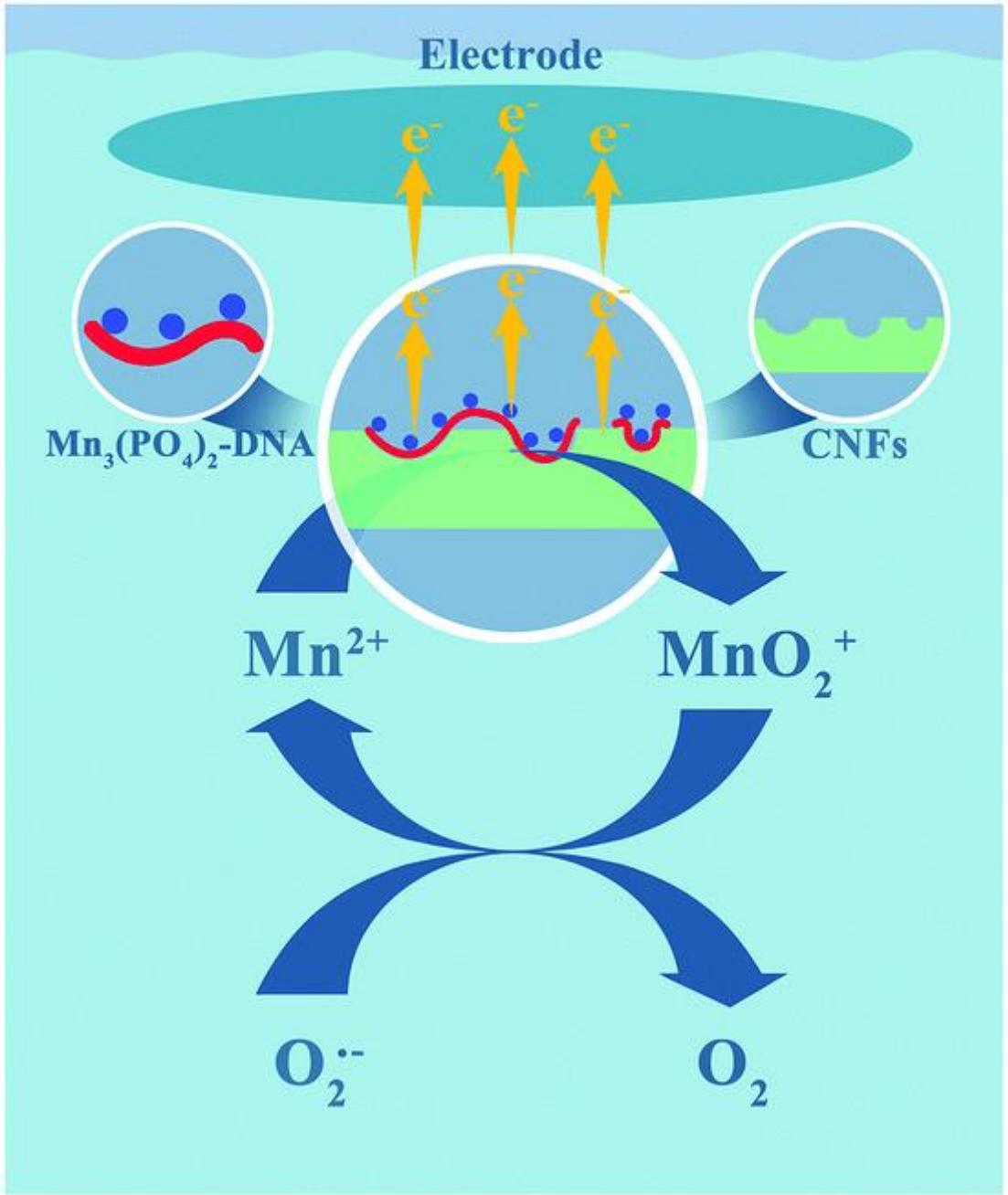

The biomimetic enzyme catalytic process.

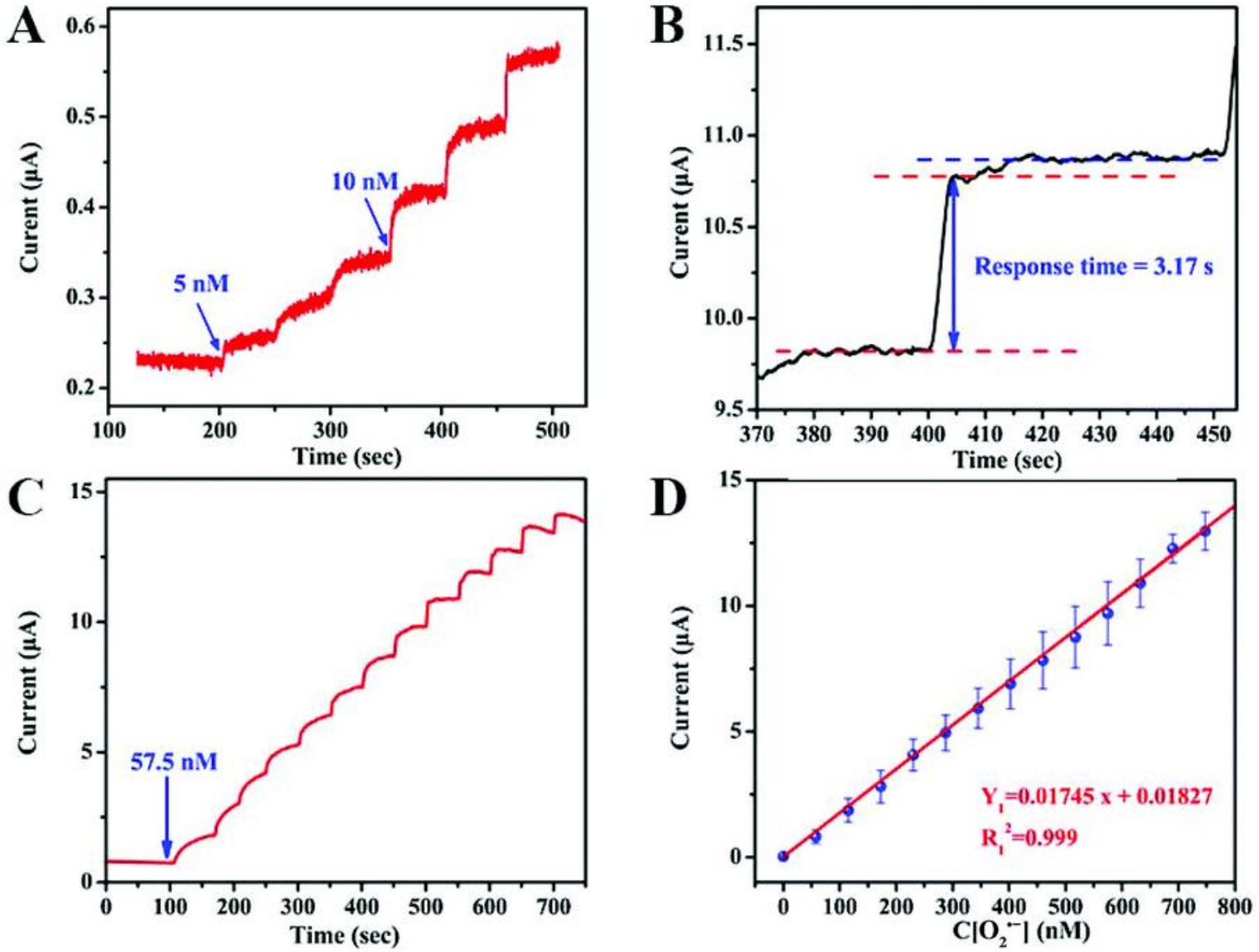

(A and C) Chronoamperometric response of the $Mn_3(PO_4)_2$–DNA/CNF/GCE sensor in response to the continuous addition of 5 nmol L^{-1}, 10 nmol L^{-1} and 57.5 nmol L^{-1} $O_2^{\bullet-}$, respectively, at an applied potential of 0.72 V *versus* Hg/Hg_2Cl_2 in 0.01 mol L^{-1} PBS, (B) response time of the $Mn_3(PO_4)_2$–DNA/CNF/GCE sensor towards $O_2^{\bullet-}$, and (D) the linear plot of response *versus* $O_2^{\bullet-}$.

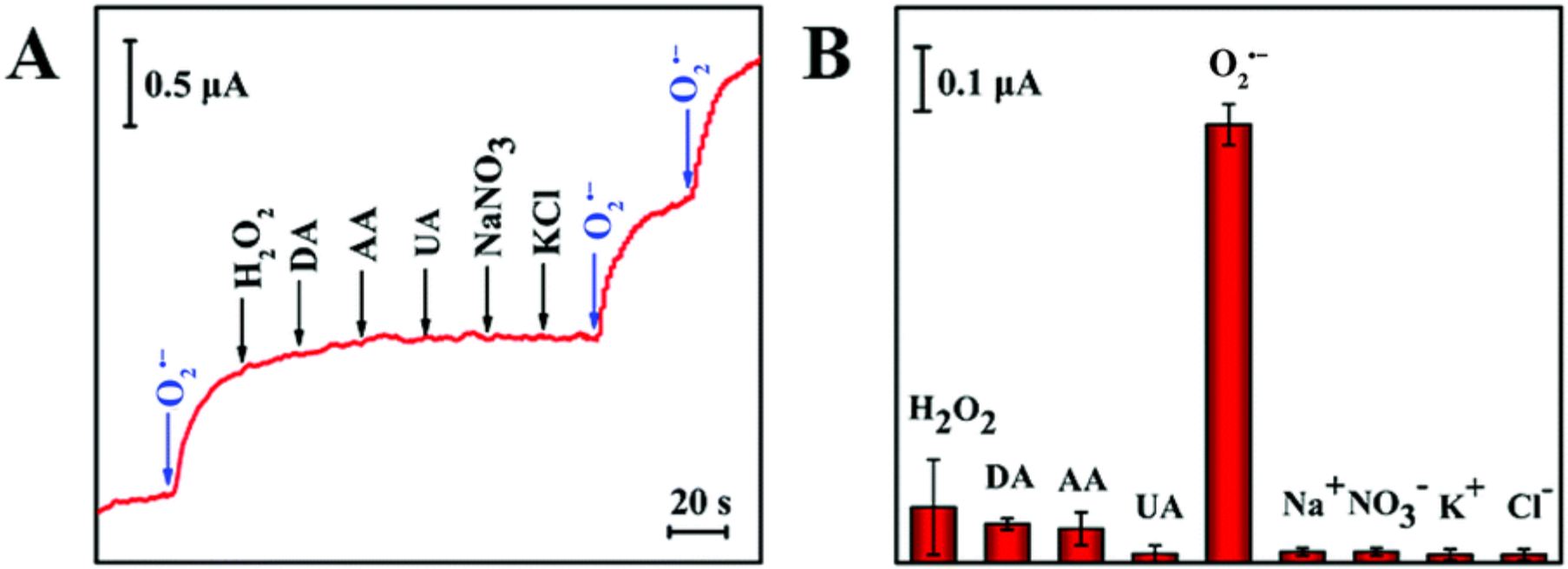

(A and B) Selective performance and histogram profile of the $Mn_3(PO_4)_2$–DNA/CNF/GCE sensor. The responses obtained on the addition of 57.5 nmol L^{-1} $O_2^{\bullet-}$ and Na^+, NO_3^-, K^+, Cl^-, dopamine (DA), ascorbic acid (AA), and uric acid (UA) up to 10 µmol L^{-1} as well as 1 µmol L^{-1} of H_2O_2.

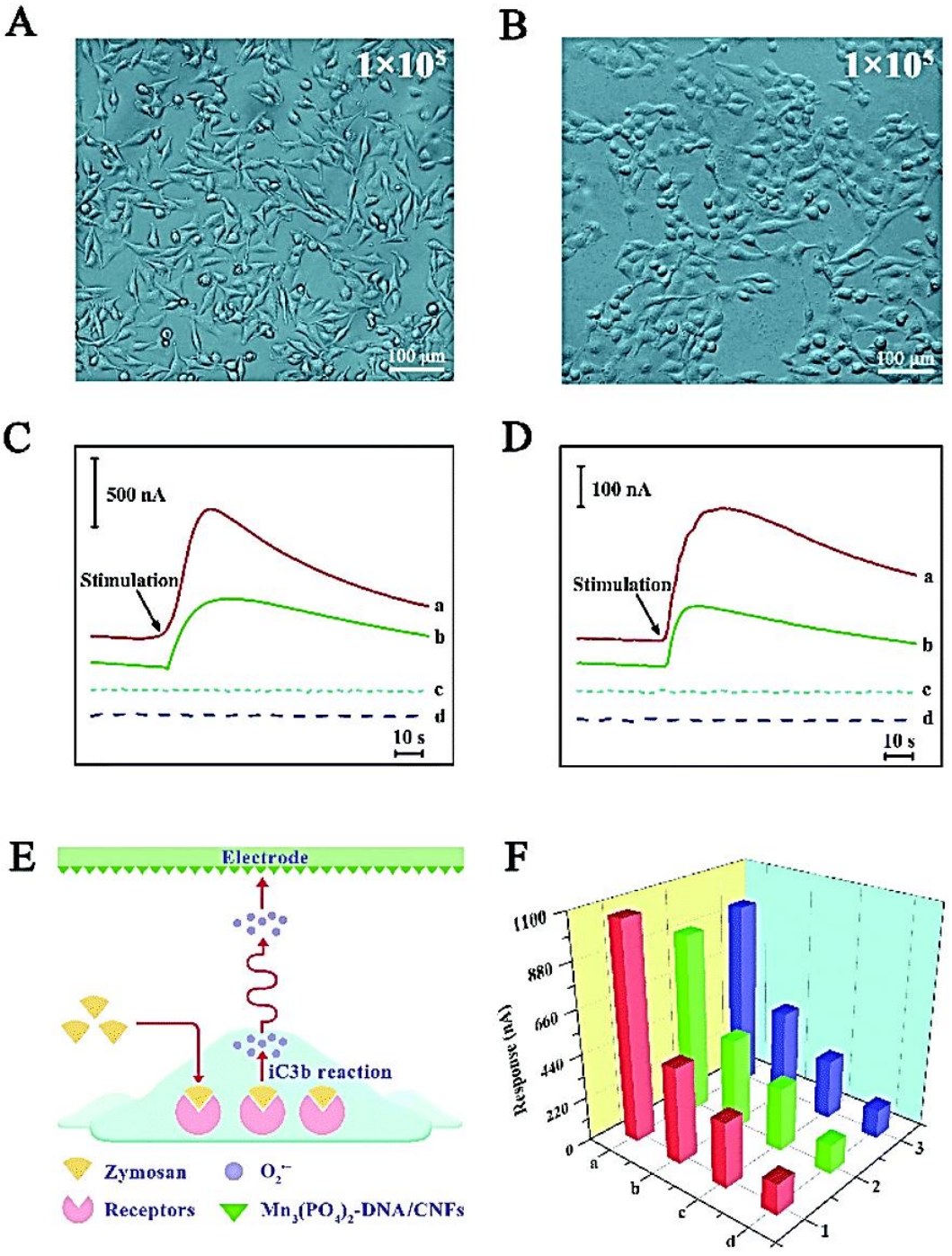

Scheme showing one path for different amounts of zymosan-triggered $O_2^{\bullet-}$ production from cells and timely capture of $O_2^{\bullet-}$ by the $Mn_3(PO_4)_2$–DNA/CNF/GCE sensor. The microscopy images of (A) A375 cells and (B) HaCaT cells with a density of 1×10^5 cells per mL. Real-time monitoring of $O_2^{\bullet-}$ released from (C) A375 cells and (D) HaCaT cells stimulated by different amounts of zymosan: (curve a) 0.2 mg mL^{-1} zymosan; (curve b) 0.1 mg mL^{-1} zymosan; (curve c) 0.1 mg mL^{-1} zymosan and SOD 300 U mL^{-1}; and (curve d) without cells, (E) one pathway for zymosan-triggered $O_2^{\bullet-}$ released from human cells and captured timely by the sensing platform, and (F) reproducibility of the sensor when detecting $O_2^{\bullet-}$ released from living cells.

Current response of $O_2^{\cdot -}$ released from cells under injection of drugs

Cell lines	Stimulation	Current [μA]
A375	0.2 mg mL^{-1} Zymosan	0.97
	0.1 mg mL^{-1} Zymosan	0.47
HaCaT	0.2 mg mL^{-1} Zymosan	0.31
	0.1 mg mL^{-1} Zymosan	0.15

Conclusion

- This work tailors the pore size distribution to fabricate a highly sensitive and selective $Mn_3(PO_4)_2$–DNA/CNF-based biomimetic enzyme sensor.
- The real-time detection of $O_2^{\bullet -}$ released from living cells is shown.
- A high mesopore ratio in the pore structure plays a critical role in the enhancement of sensitivity and selectivity.
- This highly sensitive and selective $O_2^{\bullet -}$ biomimetic enzyme sensor has a great potential in diagnosis and life science research applications